

# Orbital order from the on-site orbital attraction

M. Khodas<sup>1,2</sup> and A. V. Chubukov<sup>3</sup><sup>1</sup>*Department of Physics and Astronomy, University of Iowa, Iowa City, Iowa 52242, USA*<sup>2</sup>*Racah Institute of Physics, Hebrew University of Jerusalem, Jerusalem 91904, Israel*<sup>3</sup>*School of Physics and Astronomy, University of Minnesota, Minneapolis, Minnesota 55455, USA*

(Received 28 June 2016; revised manuscript received 9 September 2016; published 27 September 2016)

We study the model of Fe-based superconductors with intraorbital attraction, designed to favor a spontaneous orbital polarization. Previous studies of this model within the two-orbital approximation indicated that the leading instability is toward  $s$ -wave superconductivity and the subleading one is toward anti-ferro-orbital order, which breaks the translational symmetry of the crystal. The two-orbital approximation is, however, not consistent with the Fermi surface geometry of Fe superconductors, as it yields the wrong position of one of the hole pockets. Here we analyze the model with the same interaction but with realistic Fermi surface geometry (two hole pockets at the center of the Brillouin zone and two electron pockets at its boundary). We apply the parquet renormalization-group (pRG) technique to detect the leading instability upon the lowering of the temperature. We argue that the pRG analysis strongly favors a  $q = 0$  orbital order, which in the band basis is a  $d$ -wave Pomeranchuk order.

DOI: [10.1103/PhysRevB.94.115159](https://doi.org/10.1103/PhysRevB.94.115159)

## I. INTRODUCTION

The analysis of the competition and the interplay between different types of electronic order remain the key research direction in the studies of Fe-based superconductors (FeSCs) [1–5]. The three experimentally observed macroscopic orders in FeSCs are magnetism, superconductivity, and nematic order. The nematic order is less conventional than the other two, but it is ubiquitous in all known families of FeSCs and has been actively investigated in the past few years [5–9].

The nematic order breaks lattice rotational  $C_4$  symmetry down to  $C_2$  and gives rise to unequal population of  $d_{xz}$  and  $d_{yz}$  Fe orbitals and to the anisotropy of magnetic susceptibilities  $\chi_{xx} \neq \chi_{yy}$ , without breaking the spin rotational and time-reversal symmetry. The imbalance in the orbital population may or may not be accompanied by the breaking of the translational invariance of the crystal ( $q = 0$  orbital order or finite  $q$  orbital order, respectively). In the band basis, a  $q = 0$  order is a zero-momentum  $d$ -wave order in the particle-hole channel.

The origin of the nematic order remains the subject of debates. In many FeSCs, it is likely associated with partial melting of stripe magnetism [10–17]. In FeSe, however, the nematic order is not followed by a stripe magnetic order, and it may be the result of a spontaneous symmetry breaking between  $d_{xz}$  and  $d_{yz}$  orbitals [18–23]. Interestingly, the nematic order in FeSe emerges at  $T_n = 85$  K, well above superconducting  $T_c \sim 8$  K. To clarify the role of the orbital degrees of freedom in nematicity and the interplay between nematicity and superconductivity and other potential orders, it is useful to study the models in which a spontaneous orbital order is explicitly favored by the interaction. The simplest model of this kind is a two-orbital ( $d_{xz}/d_{yz}$ ) model with on-site intraorbital attraction and interorbital repulsion, tailored to favor nonequal density of fermions on  $d_{xz}$  and  $d_{yz}$  orbitals. The tight-binding fermionic dispersion in this model is obtained from the full five-orbital tight-binding dispersion by keeping only  $d_{xz}$  and  $d_{yz}$  orbitals. The two-orbital model has been studied within the random-phase approximation (RPA) (Refs. [24,25]) by weak-coupling logarithmical perturbation theory [26] and by

the Quantum Monte Carlo method (Ref. [27]). The outcome is that the two leading instabilities are the ordinary  $s$ -wave superconductivity and the  $q = (\pi, \pi)$  orbital order. At weak coupling, superconductivity wins. At larger couplings, the  $(\pi, \pi)$  orbital order may develop first. The two-orbital model is not, however, directly applicable to FeSCs because it places one of the hole Fermi surfaces in the wrong place in the Brillouin zone (BZ)—at  $(\pi, \pi)$  instead of  $(0, 0)$  1FeBZ.

In this paper, we consider the model with the same interaction, but with more realistic band structure with two hole pockets centered at  $(0, 0)$  and two electron pockets centered at  $(\pi, 0)$  and  $(0, \pi)$  in the 1FeBZ. The goal of our study is to analyze the interplay between superconductivity (SC) and  $q = 0$  orbital order, and also spin-density-wave (SDW) and charge-density-wave (CDW) orders. Several groups have argued [28–32] that to adequately describe the interplay between different ordering tendencies, one has to include into consideration the orbital composition of the low-energy excitations and analyze how different interaction channels affect each other. To do this, we apply the parquet renormalization-group technique (pRG). This technique is adequate for FeSCs because the interactions between fermions with intermediate energies  $W \gg E \gg E_F$ , where  $W$  is of order of bandwidth, are logarithmic not only in the particle-particle (Cooper) channel, but also in the particle-hole channel at momenta  $(\pi, 0)$  and  $(0, \pi)$ , due to opposite signs of the dispersions near the hole and electron pockets. Because the distance between the hole and electron pockets in momentum space is half of the reciprocal-lattice vector, a composite effect of two particle-hole excitations gives rise to a logarithmic enhancement of the interaction also in the  $q = 0$  Pomeranchuk channel. In the situation when renormalizations of the interactions in more than one channel are logarithmical, the most log-divergent Feynman graphs are known as parquet diagrams. The solution of the pRG equations amounts to the summation of all such diagrams. Physically, pRG equations show how different couplings and susceptibilities in various channels evolve as one progressively integrates out high-energy fluctuations. In all cases studied, the susceptibilities in several channels increase under pRG and diverge at some RG scale  $L = \log W/E$ , where  $E$  is

the running energy. The instability develops in the channel in which the susceptibility diverges at the highest energy (i.e., the smallest  $L = L_0 = \log W/E_0$ ). The instability temperature is of order  $E_0$ . If susceptibilities in several channels diverge at the same  $L = L_0$ , the most likely outcome is that the order develops in the channel whose susceptibility diverges with the largest exponent. This reasoning works when  $E_0 > E_F$ , i.e., when the instability develops before the scale of  $E_F$  is reached. Below  $E = E_F$ , different channels effectively decouple. Hence, if  $E_0 < E_F$ , one should run pRG down to  $E = E_F$ , obtain the values of the couplings at this scale, and then independently consider different channels (say, within the RPA) using the couplings at  $E = E_F$  as the “bare” couplings.

In our previous work [33] the two of us and R. Fernandes applied pRG technique to apply the pRG technique to the four-pocket model with repulsive intrapocket and inter-pocket interactions. We found that at intermediate energies, the largest susceptibility is in the SDW channel, the one in the  $s^{+-}$  SC channel is subleading, and the susceptibility in the orbital order channel is much smaller than the other two. However, at smaller energies the SDW and SC channels strongly compete with each other. The SC susceptibility eventually gets larger than the one in the SDW channel and diverges at the RG scale  $L = L_0$  as  $\chi_{SC} \propto (L_0 - L)^{-\alpha_{SC}}$ , where  $L = \log W/E$ , and  $E$  is the running energy. However, due to competition with SDW, the exponent  $\alpha_{SC}$  is smaller than its would-be BCS value. This reduction of the exponent paves the way for the “secondary” channels, such as the orbital order channel (the  $d$ -wave Pomeranchuk channel in the band basis), which also becomes attractive due to a push from spin fluctuations, but it does not get weakened due to competition with the SDW. The susceptibility in the  $d$ -wave Pomeranchuk channel  $\chi_P$  is smaller than  $\chi_{SC}$  at intermediate energies because the bare Pomeranchuk susceptibility is nonlogarithmic, but it may eventually diverge with the exponent  $\alpha_P > \alpha_{SC}$ . We found that this is what actually happens. Namely, the  $d$ -wave Pomeranchuk susceptibility  $\chi_P$  diverges with the exponent  $\alpha_P = 1$  and becomes the largest near  $L = L_0$ . As a result, within one-loop pRG, the leading instability upon the lowering of  $T$  is toward a spontaneous orbital order. This scenario is a plausible one for FeSe [33], however it cannot be rigorously justified for the four-pocket model because there  $\alpha_{SC}$  is not particularly small, and  $\chi_P$  becomes larger than  $\chi_{SC}$  only in the vicinity of  $L_0$ , where the running couplings are of order 1 and the corrections to one-loop pRG equations are also of order 1.

In this paper, we report the results of pRG analysis of the same model as in Ref. [33] but with intrapocket attraction. We show that in this model,  $s$ -wave and  $d$ -wave SC channels, the SDW channel, and the CDW channel are degenerate, and the susceptibilities in all these channels diverge with the same exponent,  $\chi \propto 1/(L_0 - L)^\alpha$ . Because of the competition between many channels,  $\alpha$  turns out to be very small:  $\alpha = (\sqrt{5} - 2)/3 \approx 0.08$ . As a result, these susceptibilities barely diverge. Meanwhile, the susceptibility in the Pomeranchuk channel still diverges with the exponent  $\alpha_P = 1$ . Because of the large difference in the values of the exponents, the susceptibility in the Pomeranchuk channel becomes the largest at smaller  $L$ , where one-loop pRG is under better control. In other words, the fierce competition between the two SC channels, the SDW channel, and the CDW channel nearly

halts the divergencies of the corresponding susceptibilities and allows the Pomeranchuk channel to emerge as a clear winner. These results differ from the earlier studies of a two-orbital model where the Pomeranchuk instability was found to be subleading [26,27]. This can be traced to the competition between the channels described above that is absent in the previously studied model. The Pomeranchuk instability dominates in the present case since the correlations in other channels are suppressed.

The paper is organized as follows. In Sec. II we introduce our model and discuss approximations. In Sec. III we introduce superconducting, SDW, CDW, and nematic (Pomeranchuk) order parameters, and we analyze the development and hierarchy of different types of order within the RPA, i.e., without the inclusion of the couplings between different channels. In Sec. IV we include interchannel couplings and analyze the flow of the interactions within pRG. In Sec. V we reexamine the hierarchy of instabilities by evaluating the susceptibilities in different channels along the fixed trajectories of the pRG flow. We present our conclusions in Sec. VI.

## II. THE MODEL WITH INTRAORBITAL ATTRACTION

The model we study is defined by the Hamiltonian

$$\mathcal{H} = \mathcal{H}_0 + \mathcal{H}_{\text{int}}, \quad (1)$$

where  $\mathcal{H}_0$  is the quadratic part and  $\mathcal{H}_i$  is the interaction Hamiltonian. We discuss the effective low-energy band-structure model captured by the  $\mathcal{H}_0$  first. We consider the 1FeBZ with the two hole pockets at the BZ center and the two electron pockets centered at  $\mathbf{Q}_1 = (0, \pi)$  and  $\mathbf{Q}_2 = (\pi, 0)$ . As in Ref. [33], we treat the two hole pockets as consisting of  $d_{xz}$  and  $d_{yz}$  orbitals (as they actually are), and we approximate the electron pocket at  $(0, \pi)$  as consisting of the  $d_{yz}$  orbital and the one at  $(\pi, 0)$  as consisting of the  $d_{xz}$  orbital, i.e., we neglect the contributions to electron pockets from the  $d_{xy}$  orbital.

The quadratic part of the Hamiltonian is expressed as follows:

$$\begin{aligned} \mathcal{H}_0 = \sum_{\mathbf{k}, \alpha} \sum_{\mu, \nu=1,2} & [d_{\mu\alpha}^\dagger(\mathbf{k}) \mathcal{H}_{\mu, \nu}^\Gamma(\mathbf{k}) d_{\nu\alpha}(\mathbf{k}) \\ & + f_{\mu\alpha}^\dagger(\mathbf{k}) \mathcal{H}_{\mu, \nu}^M(\mathbf{k}) f_{\nu\alpha}(\mathbf{k})], \end{aligned} \quad (2)$$

where the subscripts  $\mu, \nu = 1, 2$  refer to the  $xz$  and  $yz$  orbitals, respectively, and

$$\mathcal{H}^\Gamma(\mathbf{k}) = \begin{bmatrix} \epsilon_h + \frac{k^2}{2m_h} + ak^2 \cos 2\theta_k & ck^2 \sin 2\theta_k \\ ck^2 \sin 2\theta_k & \epsilon_h + \frac{k^2}{2m_h} - ak^2 \cos 2\theta_k \end{bmatrix} \quad (3)$$

for states near hole pockets, and

$$\mathcal{H}^M(\mathbf{k}) = \begin{bmatrix} \epsilon_e + \frac{k^2}{2m_e} + bk^2 \cos 2\theta_k & 0 \\ 0 & \epsilon_e + \frac{k^2}{2m_e} - bk^2 \cos 2\theta_k \end{bmatrix} \quad (4)$$

for states near electron pockets [34]. In Eqs. (3) and (4),  $\theta_k = \arctan(k_y/k_x)$ . The parameters  $\epsilon_{h,e}$ ,  $1/m_{h,e}$ ,  $a$ ,  $b$ , and  $c$  can be either determined by comparison with the band-structure calculations or, preferably, taken from experiments.

To simplify the calculations, we set  $a = c$  in Eq. (3), in which case the two hole FSs are circular, and the dispersions of the two hole excitations are  $\epsilon_h + k^2/(2m_{h1})$  and  $\epsilon_h + k^2/(2m_{h2})$ , where  $m_{h1,2} = m_h/(1 \pm 2am_h)$ . To simplify the presentation of the pRG results, below we neglect the difference between the two hole masses, i.e., we approximate  $m_{h1,2} \approx m_h$ . We will also neglect the  $b$  term in Eq. (4). We verified that keeping  $m_{h1}$  and  $m_{h2}$  different complicates the formulas for pRG flow, but it does not affect the results.

We now turn to the interaction Hamiltonian. We follow Refs. [24–27] and consider four-fermion interaction tailored to favor a spontaneous orbital polarization:

$$\mathcal{H}_{\text{int}} = -g \sum_j (n_{j,xz} - n_{j,yz})^2, \quad (5)$$

where the summation index  $j$  enumerates the iron sites located at  $\mathbf{R}_j$ . The orbital occupation  $n_{j,\mu}$  with  $\mu = xz, yz$  includes contributions from the two spin orientations,  $n_{j,\mu} = n_{j,\mu\uparrow} + n_{j,\mu\downarrow}$ . For each spin polarization,  $\sigma = \uparrow, \downarrow$ , the occupation  $n_{j,\mu\sigma} = \psi_{j\mu\sigma}^\dagger \psi_{j\mu\sigma}$ , where

$$\psi_{j\mu\sigma} = \frac{1}{\sqrt{N}} \sum_{\mathbf{k}} [d_{\mu\sigma}(\mathbf{k}) + f_{\mu\sigma}(\mathbf{k}) e^{i\mathbf{Q}_{1(2)} \cdot \mathbf{R}_j}] e^{i\mathbf{k} \cdot \mathbf{R}_j} \quad (6)$$

annihilates the electron at the site  $\mathbf{R}_j$  with spin  $\sigma$  in the orbital state  $\mu$ .

The Hamiltonian (5) is a particular realization of the Hubbard-Hund on-site interaction Hamiltonian,

$$\begin{aligned} H_{UJ} = & \frac{U}{2} \sum_{j,\mu} n_{j,\mu} n_{j,\mu} + \frac{U'}{2} \sum_{j,\mu \neq \mu'} n_{j,\mu} n_{j,\mu'} \\ & + \frac{J}{2} \sum_{j,\mu' \neq \mu} \sum_{\sigma\sigma'} \psi_{j\mu\sigma}^\dagger \psi_{j\mu'\sigma'}^\dagger \psi_{j\mu\sigma} \psi_{j\mu'\sigma'} \\ & + \frac{J'}{2} \sum_{j,\mu' \neq \mu} \psi_{j\mu\sigma}^\dagger \psi_{j\mu'\sigma'}^\dagger \psi_{j\mu'\sigma'} \psi_{j\mu\sigma} \end{aligned} \quad (7)$$

with

$$U = -2g, \quad U' = 2g, \quad J = J' = 0. \quad (8)$$

As we discuss below, the actual number of independent interaction constants is higher than one. As a result, few interaction channels are degenerate for the model specified by Eq. (5). For instance, as  $J' = 0$ , the pairing processes for  $d_{xz}$ - and  $d_{yz}$ -derived Cooper pairs are independent, which makes the  $s$ - and  $d$ -wave superconducting pairing degenerate. We furthermore expect the degeneracy between interorbital SDW and CDW channels as in this case the direct process contributions of Eq. (5) are absent regardless of the state of spin polarization of interacting electrons. These expectations are confirmed by explicit evaluation in Sec. III.

The original interaction Hamiltonian has just one coupling  $g$ , and one may think that one needs just one pRG equation for the flow of  $g$ . However, earlier pRG studies of FeSCs already indicated that this is not the case for two reasons. First, under pRG,  $U$  and  $U'$  become nonequivalent, and  $J$  and  $J'$  are generated. Second, the full on-site interaction Hamiltonian does not remain invariant under pRG, i.e., new interactions are generated, which can be identified as interactions between

fermions at neighboring sites. One can make sure (see Ref. [33] for details) that the total number of different  $C_4$ -symmetric four-fermion combinations of low-energy fermions from Eq. (2) is equal to 14. The corresponding Hamiltonian is

$$H = \sum_{j=1}^5 H_{U_j}, \quad (9)$$

where

$$\begin{aligned} H_{U_1} = & U_1 \sum' [f_{1\sigma}^\dagger f_{1\sigma} d_{1\sigma'}^\dagger d_{1\sigma'} + f_{2\sigma}^\dagger f_{2\sigma} d_{2\sigma'}^\dagger d_{2\sigma'}] \\ & + \bar{U}_1 \sum' [f_{2\sigma}^\dagger f_{2\sigma} d_{1\sigma'}^\dagger d_{1\sigma'} + f_{1\sigma}^\dagger f_{1\sigma} d_{2\sigma'}^\dagger d_{2\sigma'}], \end{aligned} \quad (10)$$

$$\begin{aligned} H_{U_2} = & U_2 \sum' [f_{1\sigma}^\dagger d_{1\sigma} d_{1\sigma'}^\dagger f_{1\sigma'} + f_{2\sigma}^\dagger d_{2\sigma} d_{2\sigma'}^\dagger f_{2\sigma'}] \\ & + \bar{U}_2 \sum' [f_{1\sigma}^\dagger d_{2\sigma} d_{2\sigma'}^\dagger f_{1\sigma'} + f_{2\sigma}^\dagger d_{1\sigma} d_{1\sigma'}^\dagger f_{2\sigma'}], \end{aligned} \quad (11)$$

$$\begin{aligned} H_{U_3} = & \frac{U_3}{2} \sum' [f_{1\sigma}^\dagger d_{1\sigma} f_{1\sigma'}^\dagger d_{1\sigma'} + f_{2\sigma}^\dagger d_{2\sigma} f_{2\sigma'}^\dagger d_{2\sigma'} + \text{H.c.}] \\ & + \frac{\bar{U}_3}{2} \sum' [f_{1\sigma}^\dagger d_{2\sigma} f_{1\sigma'}^\dagger d_{2\sigma'} + f_{2\sigma}^\dagger d_{1\sigma} f_{2\sigma'}^\dagger d_{1\sigma'} + \text{H.c.}], \end{aligned} \quad (12)$$

$$\begin{aligned} H_{U_4} = & \frac{U_4}{2} \sum' [d_{1\sigma}^\dagger d_{1\sigma} d_{1\sigma'}^\dagger d_{1\sigma'} + d_{2\sigma}^\dagger d_{2\sigma} d_{2\sigma'}^\dagger d_{2\sigma'}] \\ & + \frac{\bar{U}_4}{2} \sum' [d_{1\sigma}^\dagger d_{2\sigma} d_{1\sigma'}^\dagger d_{2\sigma'} + d_{2\sigma}^\dagger d_{1\sigma} d_{2\sigma'}^\dagger d_{1\sigma'}] \\ & + \tilde{U}_4 \sum' d_{1\sigma}^\dagger d_{1\sigma} d_{2\sigma'}^\dagger d_{2\sigma'} + \tilde{\bar{U}}_4 \sum' d_{1\sigma}^\dagger d_{2\sigma} d_{2\sigma'}^\dagger d_{1\sigma'}, \end{aligned} \quad (13)$$

$$\begin{aligned} H_{U_5} = & \frac{U_5}{2} \sum' [f_{1\sigma}^\dagger f_{1\sigma} f_{1\sigma'}^\dagger f_{1\sigma'} + f_{2\sigma}^\dagger f_{2\sigma} f_{2\sigma'}^\dagger f_{2\sigma'}] \\ & + \frac{\bar{U}_5}{2} \sum' [f_{1\sigma}^\dagger f_{2\sigma} f_{1\sigma'}^\dagger f_{2\sigma'} + f_{2\sigma}^\dagger f_{1\sigma} f_{2\sigma'}^\dagger f_{1\sigma'}] \\ & + \tilde{U}_5 \sum' f_{1\sigma}^\dagger f_{1\sigma} f_{2\sigma'}^\dagger f_{2\sigma'} + \tilde{\bar{U}}_5 \sum' f_{1\sigma}^\dagger f_{2\sigma} f_{2\sigma'}^\dagger f_{1\sigma'}. \end{aligned} \quad (14)$$

In Eqs. (10)–(14), the notation  $\sum'$  stands for the summation over spins and over the momenta subject to the momentum conservation. For instance,

$$\begin{aligned} \sum' f_{1\sigma}^\dagger f_{1\sigma} d_{1\sigma'}^\dagger d_{1\sigma'} &= \sum_{\mathbf{k}_1, \mathbf{k}_2, \mathbf{k}_3, \mathbf{k}_4} \sum_{\sigma, \sigma'} f_{1\sigma}^\dagger(\mathbf{k}_1) f_{1\sigma}(\mathbf{k}_2) d_{1\sigma'}^\dagger(\mathbf{k}_3) d_{1\sigma'}(\mathbf{k}_4) \\ &\times \delta_{\mathbf{k}_1 + \mathbf{k}_2 + \mathbf{k}_3 + \mathbf{k}_4, 0}, \end{aligned} \quad (15)$$

where  $\delta$  in the last line stands for the Kronecker  $\delta$ .

At the bare level,

$$\begin{aligned} U_1 = U_2 = U_3 = U_4 = U_5 &= -2g, \\ \bar{U}_1 = \bar{U}_4 = \bar{U}_5 &= 2g, \end{aligned} \quad (16)$$

and other interactions are zero. Generally, however, all 14 interactions are generated under pRG, i.e., the full set of pRG

equations contains 14 coupled equations. One can easily make sure that no other terms are generated by pRG.

Because pRG calculations involve fermions near hole and electron pockets, it is advantageous to move to the band basis, i.e., diagonalize the quadratic Hamiltonian for excitations near hole pockets and reexpress the interaction Hamiltonian in terms of band operators. We refrain from presenting the corresponding Hamiltonian, as the formula for it is quite lengthy.

### III. ORDER PARAMETERS AND SUSCEPTIBILITIES WITHIN THE RPA

We begin the discussion of potential ordered states in the model of Eq. (5) by first treating all channels as independent and analyzing the corresponding susceptibilities within the RPA. To avoid complex formulas, we present the order parameters in the orbital basis and list the results of the computations of the susceptibilities within the RPA. The actual computations of the susceptibilities were performed in the band basis.

#### A. SDW channels

There are two SDW orders with momenta  $(0, \pi)$  and  $(\pi, 0)$ . One involves bilinear combinations of fermions from the same orbital, while the other involves fermions from different orbitals.

The two intraorbital SDW order parameters are constructed of  $f_\alpha^\dagger d_\alpha$ , which are diagonal in the orbital index:

$$\begin{aligned} s_{1,2}^r &= f_{1,2}^\dagger \sigma d_{1,2} + d_{1,2}^\dagger \sigma f_{1,2}, \\ s_{1,2}^i &= i(f_{1,2}^\dagger \sigma d_{1,2} - d_{1,2}^\dagger \sigma f_{1,2}). \end{aligned} \quad (17)$$

We will refer to  $s_{1,2}^r$  and  $s_{1,2}^i$  as real and imaginary SDW order parameters. The real  $s_{1,2}^r$  gives rise to a SDW on Fe sites, and  $s_{1,2}^i$  gives rise to a spin current.

The interorbital antiferromagnetism is described by the order parameters

$$\begin{aligned} \bar{s}_{1,2}^r &= f_{1,2}^\dagger \sigma d_{2,1} + d_{1,2}^\dagger \sigma f_{2,1}, \\ \bar{s}_{1,2}^i &= i(f_{1,2}^\dagger \sigma d_{2,1} - d_{1,2}^\dagger \sigma f_{2,1}), \end{aligned} \quad (18)$$

which are off-diagonal in the orbital index. The real  $\bar{s}_{1,2}^r$  gives rise to an unconventional SDW, which in real space is concentrated on pnictogen/chalcogen sites and has no weight on Fe sites, and  $\bar{s}_{1,2}^i$  gives rise to a corresponding spin current.

The part of the interaction Hamiltonian (9), bilinear in SDW order parameter, is

$$\begin{aligned} H_{s,\pi} &= \frac{1}{8}(-U_1 - U_3)[s_1^r s_1^r + s_2^r s_2^r] \\ &\quad + \frac{1}{8}(-U_1 + U_3)[s_1^i s_1^i + s_2^i s_2^i] \\ &\quad + \frac{1}{8}(-\bar{U}_1 - \bar{U}_3)[\bar{s}_1^r \bar{s}_1^r + \bar{s}_2^r \bar{s}_2^r] \\ &\quad + \frac{1}{8}(-\bar{U}_1 + \bar{U}_3)[\bar{s}_1^i \bar{s}_1^i + \bar{s}_2^i \bar{s}_2^i]. \end{aligned} \quad (19)$$

At the bare level, the interaction between  $s_{1,2}^r$  is repulsive:  $(-U_1 - U_3)/8 = g/2 > 0$ , while the interaction between  $s_{1,2}^i$  vanishes. The interactions between  $\bar{s}_{1,2}^r$  and between  $\bar{s}_{1,2}^i$  are attractive and have the same magnitude:  $(-\bar{U}_1 \mp \bar{U}_3)/8 =$

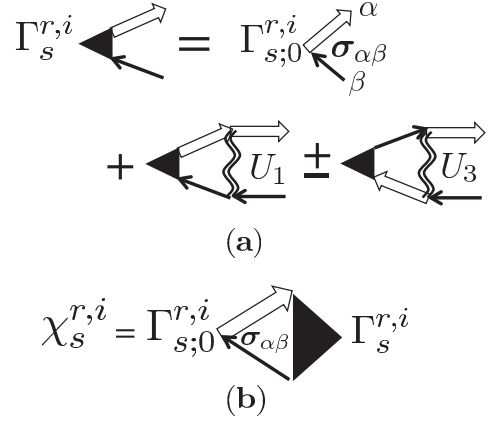


FIG. 1. (a) Graphical representation of the Dyson equation for the vertices  $\Gamma_s$  in the SDW channel. Equation (20) for  $\bar{\Gamma}_s$  is obtained by replacing all  $U_i$  by  $\bar{U}_i$ . Single (double) lines represent propagators of fermions near hole (electron) pockets. (b) Graphical representation of the RPA formula for the susceptibility in the spin channel, Eq. (23).

$-g/4 < 0$ . Adding the terms  $\bar{\Gamma}_{s;0} s_{1,2}^{r,i}$  with infinitesimally small prefactors  $\bar{\Gamma}_{s;0}$  to the Hamiltonian and summing up ladder series of renormalizations of  $\bar{\Gamma}$ , we obtain [see Fig. 1(a)]

$$\bar{\Gamma}_{s;1,2}^{r,i} = \frac{\bar{\Gamma}_{s;0}}{1 - 2\bar{g} \log W/T}, \quad (20)$$

where we introduced

$$\bar{g} = \frac{gm}{4\pi} \quad (21)$$

with  $m = 2m_h m_e / (m_h + m_e)$ , and  $m_h$  and  $m_e$  are the masses for excitations near hole and electron pockets; see Eqs. (3) and (4) and the discussion after them.

Equation (20) holds for  $T$  larger than a typical energy below which the logarithm in the particle-hole channel at momenta  $(0, \pi)$  and  $(\pi, 0)$  is cut (Ref. [35]). We see that, within the RPA, interorbital magnetic instability develops at the temperature  $T_{\text{SDW}}$  at which

$$2\bar{g} \log \frac{W}{T_{\text{SDW}}} = 1. \quad (22)$$

The same result can be obtained by analyzing the susceptibilities within the RPA. The bare susceptibilities in  $s_{1,2}^{r,i}$  channels are  $\chi_0(T) = (2m/\pi) \log W/T$ . Within the RPA, the full susceptibilities in  $s_{1,2}^{r,i}$  channels are [see Fig. 1(b)]

$$\bar{\chi}_{s;1,2}^{r,i}(T) = \frac{\chi_0(T)}{1 - (g/4)\chi_0(T)} = \frac{\chi_0(T)}{1 - 2\bar{g} \log W/T}. \quad (23)$$

The susceptibilities obviously diverge at the same  $T_{\text{SDW}}$  as the vertices  $\bar{\Gamma}_{1,2}^{r,i}$ .

#### B. CDW channels

We next consider CDW order parameters with momenta  $(\pi, 0)$  and  $(0, \pi)$ . As in the SDW case, we have two types of order parameters: diagonal and nondiagonal in the orbital index. The order parameters diagonal in the orbital index

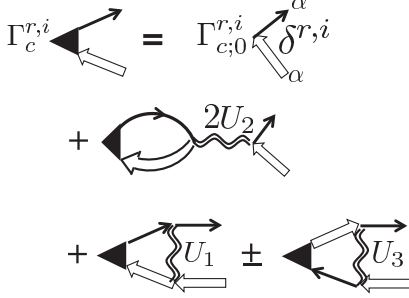


FIG. 2. Graphical representation of the Dyson equation for the vertices,  $\Gamma_c$ , in the CDW channel. The infinitesimal external perturbation giving rise to the vertex is proportional to  $\delta^{r,i}$  introduced in Eq. (24), which is diagonal in spin indices. Equation (27) for  $\bar{\Gamma}_s$  is obtained by replacing all  $U_i$  by  $\bar{U}_i$  and  $\delta^{r,i}$  by  $\bar{\delta}^{r,i}$ .

are

$$\begin{aligned}\delta_{1,2}^r &= f_{1,2}^\dagger d_{1,2} + d_{1,2}^\dagger f_{1,2}, \\ \delta_{1,2}^i &= i(f_{1,2}^\dagger d_{1,2} - d_{1,2}^\dagger f_{1,2}),\end{aligned}\quad (24)$$

and the ones nondiagonal in the orbital index are

$$\begin{aligned}\bar{\delta}_{1,2}^r &= f_{1,2}^\dagger d_{2,1} + d_{2,1}^\dagger f_{1,2}, \\ \bar{\delta}_{1,2}^i &= i(f_{1,2}^\dagger d_{2,1} - d_{2,1}^\dagger f_{1,2}).\end{aligned}\quad (25)$$

The order parameter that gives rise to the CDW on the Fe sites is  $\delta_{1,2}^r$ . The order parameter  $\bar{\delta}_{1,2}^i$  gives rise to charge current. The corresponding interaction terms, bilinear in  $\delta_{1,2}^r$  and  $\bar{\delta}_{1,2}^i$ , are

$$\begin{aligned}H_{\delta,\pi} &= \frac{1}{8}(-U_1 + 2U_2 + U_3)[\delta_1^r \delta_1^r + \delta_2^r \delta_2^r] \\ &+ \frac{1}{8}(-U_1 + 2U_2 - U_3)[\delta_1^i \delta_1^i + \delta_2^i \delta_2^i] \\ &+ \frac{1}{8}(-\bar{U}_1 + 2\bar{U}_2 + \bar{U}_3)[\bar{\delta}_1^r \bar{\delta}_1^r + \bar{\delta}_2^r \bar{\delta}_2^r] \\ &+ \frac{1}{8}(-\bar{U}_1 + 2\bar{U}_2 - \bar{U}_3)[\bar{\delta}_1^i \bar{\delta}_1^i + \bar{\delta}_2^i \bar{\delta}_2^i].\end{aligned}\quad (26)$$

Performing the same analysis as in the previous section, i.e., adding to the Hamiltonian the extra terms  $\Gamma_{c;0}\delta_{1,2}^{r,i}$  and  $\bar{\Gamma}_{c;0}\bar{\delta}_{1,2}^{r,i}$  with infinitesimally small  $\Gamma_{c;0}$  and summing up ladder diagrams for the renormalization of the vertices in  $\delta_{1,2}^{r,i}$  and  $\bar{\delta}_{1,2}^{r,i}$  channels, we find two results. First, the interaction in both interorbital CDW channels is  $(-\bar{U}_1 + 2\bar{U}_2 \pm \bar{U}_3)/8 = -g/4$ . The equation for the full vertex  $\bar{\Gamma}_{c;1,2}^{r,i}$  then has the same form as Eq. (20) for the SDW vertex; see Fig. 2:

$$\bar{\Gamma}_{c;1,2}^{r,i} = \frac{\bar{\Gamma}_{c;0}}{1 - 2\bar{g} \log W/T}. \quad (27)$$

Accordingly, the instability temperature in this channel is the same as for the interorbital SDW; see Eq. (22).

Second, the interaction in the  $\delta_{1,2}^i$  channel vanishes, and the one in the  $\delta_{1,2}^r$  channel (a conventional CDW channel) is attractive:  $(-U_1 + 2U_2 + U_3)/8 = -g/2$ . Accordingly, the vertex renormalization is given by

$$\Gamma_{c;1,2}^r = \frac{\Gamma_{c;0}}{1 - 4\bar{g} \log W/T}. \quad (28)$$

The coupling in (28) is twice as large as that in (27), hence the leading instability in the CDW subset is toward a conventional CDW order  $\delta_{1,2}^r$ . The corresponding instability temperature  $T_{\text{CDW}}$  is the solution of

$$4\bar{g} \log \frac{W}{T_{\text{CDW}}} = 1. \quad (29)$$

### C. Superconducting channels

We now turn to the Cooper channel. We introduce

$$\kappa_{\mu\mu'}^f = f_{\mu\uparrow} f_{\mu'\downarrow}, \quad \kappa_{\mu\mu'}^d = d_{\mu\uparrow} d_{\mu'\downarrow}. \quad (30)$$

and we classify fermion bilinear operators with zero total momentum via the one-dimensional irreducible representations of the  $D_{4h}$  point group  $A_{1g}$ ,  $B_{1g}$ ,  $B_{2g}$ , and  $A_{2g}$  as

$$\begin{aligned}\kappa_{A_{1g}}^{f(d)} &= \kappa_{11}^{f(d)} + \kappa_{22}^{f(d)}, \\ \kappa_{B_{1g}}^{f(d)} &= \kappa_{11}^{f(d)} - \kappa_{22}^{f(d)}, \\ \kappa_{B_{2g}}^{f(d)} &= \kappa_{12}^{f(d)} + \kappa_{21}^{f(d)}, \\ \kappa_{A_{2g}}^{f(d)} &= \kappa_{12}^{f(d)} - \kappa_{21}^{f(d)}.\end{aligned}\quad (31)$$

The subscript  $g$  in the labels implies that the order parameters are even under inversion. The  $A_{2g}$  combination vanishes for a singlet pairing because it is odd in the orbital indices.

The interaction terms bilinear in  $\kappa$  are obtained from Eq. (9) by setting the momenta of the two creation operators appearing in each separate term in Eqs. (10)–(14) to be opposite. [See Eq. (15) for the explicit definition of these terms.] The resulting interaction decouples between different symmetries:

$$H_\kappa = H_{\kappa_{A_1}} + H_{\kappa_{B_1}} + H_{\kappa_{B_2}}. \quad (32)$$

Each term in Eq. (32) is expressed through the bilinear components, Eq. (31), as

$$\begin{aligned}H_{\kappa_{A_1}} &= \frac{1}{2}(U_5 + \bar{U}_5)[\kappa_{A_1}^f]^\dagger \kappa_{A_1}^f + \frac{1}{2}(U_4 + \bar{U}_4)[\kappa_{A_1}^d]^\dagger \kappa_{A_1}^d \\ &+ \frac{1}{2}(U_3 + \bar{U}_3)([\kappa_{A_1}^f]^\dagger \kappa_{A_1}^d + \text{H.c.}),\end{aligned}\quad (33)$$

$$\begin{aligned}H_{\kappa_{B_1}} &= \frac{1}{2}(U_5 - \bar{U}_5)[\kappa_{B_1}^f]^\dagger \kappa_{B_1}^f + \frac{1}{2}(U_4 - \bar{U}_4)[\kappa_{B_1}^d]^\dagger \kappa_{B_1}^d \\ &+ \frac{1}{2}(U_3 - \bar{U}_3)([\kappa_{B_1}^f]^\dagger \kappa_{B_1}^d + \text{H.c.}),\end{aligned}\quad (34)$$

$$H_{\kappa_{B_2}} = \frac{1}{2}(\tilde{U}_5 + \tilde{\bar{U}}_5)[\kappa_{B_2}^f]^\dagger \kappa_{B_2}^f + \frac{1}{2}(\tilde{U}_4 + \tilde{\bar{U}}_4)[\kappa_{B_2}^d]^\dagger \kappa_{B_2}^d. \quad (35)$$

In the  $B_2$  channel represented by Eq. (35), the interactions involving fermions near the hole and electron pockets decouple, and the interactions are repulsive:  $\tilde{U}_5 + \tilde{\bar{U}}_5 = \tilde{U}_4 + \tilde{\bar{U}}_4 = 2g$ . As a result, there is no SC instability in the  $B_{2g}$  channel within the RPA.

In  $A_{1g}$  ( $s$ -wave) and  $B_{1g}$  ( $d$ -wave) Cooper channels, we have, at the bare level,  $U_5 + \bar{U}_5 = U_5 - \bar{U}_5 = -2g$ ,  $U_4 + \bar{U}_4 = U_4 - \bar{U}_4 = -2g$ , and  $U_3 + \bar{U}_3 = U_3 - \bar{U}_3 = -2g$ . Comparing (33) and (34), we immediately find that  $A_{1g}$  and  $B_{1g}$  channels are degenerate. Introducing the order parameters  $\kappa_{A_{1g}}^{f(d)}$  and  $\kappa_{B_{1g}}^{f(d)}$  with the bare vertices  $\Gamma_{\text{SC};A_{1g}(B_{1g})}^{f,d} = \Gamma_{\text{SC};0}$  into the Hamiltonian, and summing up the series of

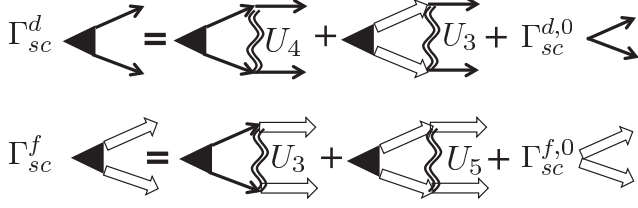


FIG. 3. Graphical representation of the Dyson equation (36) for the vertices  $\Gamma_{SC}^{f,d}$  in spin-singlet  $A_{1g}$  and  $B_{1g}$  Cooper channels. Antisymmetrization with respect to spin indices is assumed. The equations for  $A_{1g}$  and  $B_{1g}$  are the same, but the bare vertices  $\Gamma_{SC;A_{1g}(B_{1g})}^0$  and  $\Gamma_{SC;A_{1g}(B_{1g})}^0$  have different symmetry properties (both are labeled as  $\Gamma_{SC}^0$  in the figure).

ladder renormalizations (see Fig. 3), we obtain

$$\begin{aligned}\Gamma_{SC;A_{1g}(B_{1g})}^f &= -\Gamma_{SC;A_{1g}(B_{1g})}^f u_5 L - \Gamma_{SC;A_{1g}(B_{1g})}^d u_{3a} L + \Gamma_{SC}^{f,0}, \\ \Gamma_{SC;A_{1g}(B_{1g})}^d &= -\Gamma_{SC;A_{1g}(B_{1g})}^f u_{3b} L - \Gamma_{SC;A_{1g}(B_{1g})}^d u_4 L + \Gamma_{SC}^{d,0},\end{aligned}\quad (36)$$

where  $L = \log(W/T)$  is the Cooper logarithm, and the dimensionless interactions are

$$\begin{aligned}u_4 &= U_4 m_h / (4\pi), \quad u_5 = U_5 m_e / (4\pi), \\ u_{3a,b} &= U_3 m_{h,e} / (4\pi).\end{aligned}\quad (37)$$

Introducing the matrix

$$M_{SC} = -L \begin{bmatrix} u_5 & u_3 \\ u_3 & u_4 \end{bmatrix}, \quad (38)$$

we can rewrite Eq. (36) as

$$\begin{bmatrix} \Gamma_{SC;A_{1g},B_{1g}}^f \\ \Gamma_{SC;A_{1g},B_{1g}}^d \end{bmatrix} = M_{SC} \begin{bmatrix} \Gamma_{SC;A_{1g},B_{1g}}^f \\ \Gamma_{SC;A_{1g},B_{1g}}^d \end{bmatrix} + \begin{bmatrix} \Gamma_{SC;A_{1g},B_{1g}}^0 \\ \Gamma_{SC;A_{1g},B_{1g}}^0 \end{bmatrix}. \quad (39)$$

The instability occurs once the largest of the eigenvalues of the matrix  $M_{SC}$  reaches unity. There are two eigenvalues of  $M_{SC}$ , equal in  $A_{1g}$  and  $B_{1g}$  channels. In the  $A_{1g}$  channel, they describe the sign-preserving  $s$ -wave order parameter  $s^{++}$  and the order parameter  $s^{+-}$ , which changes the sign between the hole and electron Fermi surfaces. In the  $B_{1g}$  channel, the corresponding eigenvalues describe a conventional  $d$ -wave order parameter ( $d^{++}$ ) and a  $d^{+-}$  order parameter that additionally changes the sign between the hole and electron Fermi surfaces. Evaluating the eigenvalues, we immediately find that  $\lambda_{s^{++}} = \lambda_{d^{++}} > \lambda_{s^{+-}} = \lambda_{d^{+-}}$ , hence the first instability upon the lowering of  $T$  is in the  $++$  channel ( $s$ -wave or  $d$ -wave). The corresponding eigenvalue is

$$\lambda_{s^{++}} = \lambda_{d^{++}} = \left[ -(u_4 + u_5) + \sqrt{\left(\frac{u_4 - u_5}{2}\right)^2 + u_{3a} u_{3b}} \right] L. \quad (40)$$

Substituting the bare values of the couplings, we find

$$\lambda_{s^{++}} = \lambda_{d^{++}} = 4\bar{g}L. \quad (41)$$

Note that this result holds for any ratio of the masses  $m_e/m_h$ . The superconducting  $T_c$  in the  $s^{++}$  and  $d^{++}$  channels is then

determined from

$$4\bar{g} \log \frac{W}{T_c} = 1. \quad (42)$$

Comparing with Eq. (29), we find that  $T_c$  and  $T_{CDW}$  coincide, i.e., within the RPA, two superconducting channels and a conventional CDW channel are degenerate in the sense that the instability temperatures are the same in all three channels. Intraorbital SDW and CDW channels are also degenerate, but the instability temperatures in these channels are smaller.

#### D. Particle-hole channels at zero-momentum transfer

We next analyze the potential instabilities in the particle-hole channel that do not break the translational symmetry of the crystal. The corresponding order parameters involve bilinear fermion combinations

$$\rho_{\mu\mu'}^f = \sum_{\sigma} f_{\mu\sigma}^{\dagger} f_{\mu'\sigma}, \quad \rho_{\mu\mu'}^d = \sum_{\sigma} d_{\mu\sigma}^{\dagger} d_{\mu'\sigma}. \quad (43)$$

As we did for superconductivity, we classify fermion bilinear operators with zero transferred momentum via the irreducible representations of the  $D_{4h}$  point group. The combinations in (43) are even under inversion, and their transformation includes only one-dimensional irreducible representations  $A_{1g}$ ,  $B_{1g}$ ,  $B_{2g}$ , and  $A_{2g}$ . We omit subscript  $g$  below to simplify the notations.

A simple experimentation shows that the combinations of  $\rho_{\mu\mu'}^{f,d}$ , which transform as a particular representation, are

$$\begin{aligned}\rho_{A_1}^{f(d)} &= \rho_{11}^{f(d)} + \rho_{22}^{f(d)}, \\ \rho_{B_1}^{f(d)} &= \rho_{11}^{f(d)} - \rho_{22}^{f(d)}, \\ \rho_{A_2}^{f(d)} &= i(\rho_{12}^{f(d)} - \rho_{21}^{f(d)}), \\ \rho_{B_2}^{f(d)} &= \rho_{12}^{f(d)} + \rho_{21}^{f(d)}.\end{aligned}\quad (44)$$

To obtain the interactions in the particle-hole charge channel at zero-momentum transfer, we set  $\mathbf{k}_1 = \mathbf{k}_2$  or  $\mathbf{k}_1 = \mathbf{k}_4$  in Eq. (9). Expressing Eq. (9) in terms of the combinations (44), we obtain

$$H_{\rho} = H_{\rho_{A_1}} + H_{\rho_{A_2}} + H_{\rho_{B_1}} + H_{\rho_{B_2}}, \quad (45)$$

where

$$\begin{aligned}H_{\rho_{A_1}} &= \frac{1}{8}(U_5 + 2\tilde{U}_5 - \tilde{U}_5)[\rho_{A_1}^f]^2 + \frac{1}{8}(U_4 + 2\tilde{U}_4 - \tilde{U}_4)[\rho_{A_1}^d]^2 \\ &\quad + \frac{1}{4}\rho_{A_1}^f \rho_{A_1}^d (2U_1 - U_2 + 2\tilde{U}_1 - \tilde{U}_2),\end{aligned}\quad (46)$$

$$\begin{aligned}H_{\rho_{B_1}} &= \frac{1}{8}(U_5 - 2\tilde{U}_5 + \tilde{U}_5)[\rho_{B_1}^f]^2 + \frac{1}{8}(U_4 - 2\tilde{U}_4 + \tilde{U}_4)[\rho_{B_1}^d]^2 \\ &\quad + \frac{1}{4}\rho_{B_1}^f \rho_{B_1}^d (2U_1 - U_2 - 2\tilde{U}_1 + \tilde{U}_2),\end{aligned}\quad (47)$$

$$H_{\rho_{A_2}} = \frac{1}{8}(\tilde{U}_5 - 2\tilde{U}_5 + \tilde{U}_5)[\rho_{A_2}^f]^2 + \frac{1}{8}(\tilde{U}_4 - 2\tilde{U}_4 + \tilde{U}_4)[\rho_{A_2}^d]^2, \quad (48)$$

$$H_{\rho_{B_2}} = \frac{1}{8}(\tilde{U}_5 + 2\tilde{U}_5 - \tilde{U}_5)[\rho_{B_2}^f]^2 + \frac{1}{8}(\tilde{U}_4 + 2\tilde{U}_4 - \tilde{U}_4)[\rho_{B_2}^d]^2. \quad (49)$$

We consider different channels separately, each time introducing order parameters into the Hamiltonian and summing

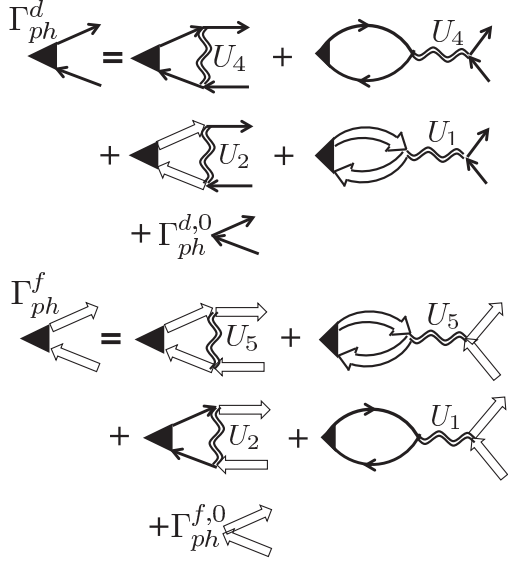


FIG. 4. Diagrammatic representation of the Dyson equation for the interaction vertices in the Pomeranchuk channels  $A_1$  and  $B_1$ , Eqs. (50) and (54). The contributions from the interactions  $\tilde{U}_{1,2}$ ,  $\tilde{U}_{4,5}$ , and  $\tilde{U}_{5,5}$ , which distinguish between  $A_1$  and  $B_1$  channels, are not shown.

up ladder series of vertex renormalizations. To simplify the formulas, below we set  $m_h = m_e$ .

### 1. $B_1$ Pomeranchuk channel

The  $B_{1g}$  order parameter  $\rho_{B_1}^{f(d)}$  changes sign under the  $C_4$  rotation. The vertices  $\Gamma_{ph;B_1}^{f(d)}$  satisfy (see Fig. 4)

$$\begin{bmatrix} \Gamma_{ph;B_1}^d \\ \Gamma_{ph;B_1}^f \end{bmatrix} = M_{ph;B_1} \begin{bmatrix} \Gamma_{ph;B_1}^d \\ \Gamma_{ph;B_1}^f \end{bmatrix} + \begin{bmatrix} \Gamma_{ph;B_1}^{d,0} \\ \Gamma_{ph;B_1}^{f,0} \end{bmatrix}, \quad (50)$$

where  $\Gamma_{ph;B_1}^{d(0)}$  and  $\Gamma_{ph;B_1}^{f(0)}$  are the bare vertices, and

$$M_{ph;B_1} = -2 \begin{bmatrix} u_4 - 2\tilde{u}_4 + \tilde{\tilde{u}}_4 & 2u_1 - 2\tilde{u}_1 - u_2 + \tilde{u}_2 \\ 2u_1 - 2\tilde{u}_1 - u_2 + \tilde{u}_2 & u_5 - 2\tilde{u}_5 + \tilde{\tilde{u}}_5 \end{bmatrix}. \quad (51)$$

Notice that there is no logarithm on the right-hand side of (51). This is a consequence of the fact that particle-hole susceptibility at zero-momentum transfer is nonlogarithmic and is just the density of states at the Fermi level.

Using the values of the bare couplings from Eqs. (16) and (37), we obtain

$$M_{ph;B_1} = 12\bar{g} \begin{bmatrix} 1 & 1 \\ 1 & 1 \end{bmatrix}. \quad (52)$$

As before, there are two eigenvalues. One corresponds to the  $d$ -wave order parameter  $n_{xz}-n_{yz}$  with the same sign on the hole and electron pockets, while for the other there is a sign change between  $n_{xz}-n_{yz}$  on the hole and electron pockets. In analogy with superconductivity, we label these order parameters as  $d_{++}$  and  $d_{+-}$ . The eigenvalues of  $M_{ph;B_1}$  are  $\lambda_{P;++} = 24\bar{g}$ ,  $\lambda_{P;+-} = 0$ . The coupling in the  $d_{++}$  channel is attractive, but because there is no logarithm, the  $B_{1g}$  Pomeranchuk instability

develops only if the coupling exceeds the critical value

$$g > g_{ph;B_1} = \frac{\pi}{6m}. \quad (53)$$

### 2. $A_1$ Pomeranchuk channel

The order parameter  $\rho_{A_1}^{f(d)}$  does not reduce the symmetry of the system, and as a result the susceptibility in this channel never truly diverges. Nevertheless, the  $A_{1g}$  susceptibility can become large, and if the corresponding order parameter changes sign between the electron and hole pockets, the enhancement of the  $A_{1g}$  susceptibility leads to simultaneous shrinking (or enhancement) of electron and hole pockets. The vertices  $\Gamma_{ph;A_1}^{d,f}$  satisfy (see Fig. 4)

$$\begin{bmatrix} \Gamma_{ph;A_1}^d \\ \Gamma_{ph;A_1}^f \end{bmatrix} = M_{ph;A_1} \begin{bmatrix} \Gamma_{ph;A_1}^d \\ \Gamma_{ph;A_1}^f \end{bmatrix} + \begin{bmatrix} \Gamma_{ph;A_1}^{d,0} \\ \Gamma_{ph;A_1}^{f,0} \end{bmatrix}, \quad (54)$$

where

$$M_{ph;A_1} = -2 \begin{bmatrix} u_4 + 2\tilde{u}_4 - \tilde{\tilde{u}}_4 & 2u_1 + 2\tilde{u}_1 - u_2 - \tilde{u}_2 \\ 2u_1 + 2\tilde{u}_1 - u_2 - \tilde{u}_2 & u_5 + 2\tilde{u}_5 - \tilde{\tilde{u}}_5 \end{bmatrix}. \quad (55)$$

The matrix  $M_{ph;A_1}$  in Eq. (55) differs from the matrix  $M_{ph;B_1}$  in Eq. (51) by signs in front of  $\tilde{u}_{4,5}$ ,  $\tilde{\tilde{u}}_{4,5}$ , and  $\tilde{u}_{1,2}$ . Substituting the bare values of the couplings from Eq. (16), we obtain

$$M_{ph;A_1} = -4\bar{g} \begin{bmatrix} 1 & 1 \\ 1 & 1 \end{bmatrix}. \quad (56)$$

We see that the matrix  $M_{ph;A_1}$  has no positive eigenvalues. As a result, there is no enhancement of the susceptibility in the  $A_{1g}$  Pomeranchuk channel.

### 3. $A_2$ and $B_2$ Pomeranchuk channels

Equations (48) and (49) show that the interaction in the  $A_{2g}$  channel is repulsive, and that in the  $B_{2g}$  channel is attractive. Analyzing the effects of the vertex renormalization in the same way as for other channels, we find that the instability in the  $B_2$  channel occurs at

$$g_{ph;B_2} = \frac{m}{4\pi}. \quad (57)$$

Comparing (53) and (57), we see that  $g_{ph;B_2} > g_{ph;B_1}$ . As a result, within the RPA, the instability in the  $d$ -wave Pomeranchuk channel occurs at a smaller coupling.

## IV. RG ANALYSIS

The existence of logarithmic renormalizations in both particle-hole and Cooper channels makes it necessary to study the coupling between the different channels. As we said in the Introduction, this can be achieved by applying the pRG technique. The pRG approach goes well beyond the RPA. In particular, it includes nonladder diagrams that describe how fluctuations in one channel affect an effective interaction in the other channel. pRG studies have been performed for pure band models with angle-independent interactions between band fermions [29–31], and recently for an orbitally projected four-pocket model with repulsive intraorbital interactions [33]. To incorporate the Pomeranchuk channels, it is crucial to

maintain the orbital content of the low-energy fermions. Our model is the same as that studied in Ref. [33], but some bare interactions are of different sign. We show that in our situation the system is in the basin of attraction of another fixed trajectory, and the system behavior is qualitatively different from that found in Ref. [33].

To simplify the presentation, we again assume that  $m_h = m_e$ . The derivation of pRG equations has been presented in Ref. [33], and we use the results of that paper.

The pRG equations are split into three groups. The two interactions  $\tilde{u}_5$  and  $\tilde{\tilde{u}}_5$  describe the subclass of scattering processes within the electron pockets. The flow of these two interactions decouples from that of other interactions and is only due to logarithmic renormalizations in the Cooper channel:

$$\begin{aligned}\dot{\tilde{u}}_5 &= -(\tilde{u}_5^2 + \tilde{\tilde{u}}_5^2), \\ \dot{\tilde{\tilde{u}}}_5 &= -2\tilde{u}_5\tilde{\tilde{u}}_5,\end{aligned}\quad (58)$$

where the derivative is with respect to  $L = \log W/E$ , and  $E$  is the running energy at which the system is probed (all couplings vary with  $L$ ). In our case, the bare value  $\tilde{\tilde{u}}_5(L=0) = 0$ . Equation (58) shows that this coupling is then not generated under pRG. The bare value of  $\tilde{u}_5(L=0)$  is  $gm/(2\pi) > 0$ . According to (58), this coupling then flows to zero under pRG.

Similarly, the two interactions involving fermions only near hole pockets also decouple and flow according to

$$\begin{aligned}\dot{\tilde{u}}_4 &= -(\tilde{u}_4^2 + \tilde{\tilde{u}}_4^2), \\ \dot{\tilde{\tilde{u}}}_4 &= -2\tilde{u}_4\tilde{\tilde{u}}_4.\end{aligned}\quad (59)$$

Again, in our model the bare values are  $\tilde{\tilde{u}}_4(L=0) = 0$  and  $\tilde{u}_4(L=0) > 0$ . According to (59),  $\tilde{\tilde{u}}_4$  is not generated, and  $\tilde{u}_4(L)$  flows to zero.

The third group of pRG equations reads

$$\begin{aligned}\dot{u}_1 &= u_1^2 + u_3^2, \quad \dot{\bar{u}}_1 = \bar{u}_1^2 + \bar{u}_3^2, \\ \dot{u}_2 &= 2u_1u_2 - 2u_2^2, \quad \dot{\bar{u}}_2 = 2\bar{u}_1\bar{u}_2 - 2\bar{u}_2^2, \\ \dot{u}_3 &= -u_3u_4 - \bar{u}_3\bar{u}_4 + 4u_3u_1 - 2u_2u_3 - u_5u_3 - \bar{u}_5\bar{u}_3, \\ \dot{\bar{u}}_3 &= -\bar{u}_3u_4 - u_3\bar{u}_4 + 4\bar{u}_3\bar{u}_1 - 2\bar{u}_2\bar{u}_3 - u_5\bar{u}_3 - \bar{u}_5\bar{u}_3, \\ \dot{u}_4 &= -u_4^2 - \bar{u}_4^2 - u_3^2 - \bar{u}_3^2, \\ \dot{\bar{u}}_4 &= -2u_4\bar{u}_4 - 2u_3\bar{u}_3, \\ \dot{u}_5 &= -u_5^2 - \bar{u}_5^2 - u_3^2 - \bar{u}_3^2, \\ \dot{\bar{u}}_5 &= -2u_5\bar{u}_5 - 2u_3\bar{u}_3.\end{aligned}\quad (60)$$

In our model,  $\bar{u}_i(L=0) = 0, i = 2, 3, 4, 5$ . Because the derivative  $\dot{\bar{u}}_i$  is proportional to  $\bar{u}_i$ , the running  $\bar{u}_i(L)$  simply remain zero:

$$\bar{u}_i(L) = 0, \quad i = 2 - 5. \quad (61)$$

With this simplification, the equation for  $\bar{u}_1$  also decouples from the rest and becomes

$$\dot{\bar{u}}_1 = \bar{u}_1^2. \quad (62)$$

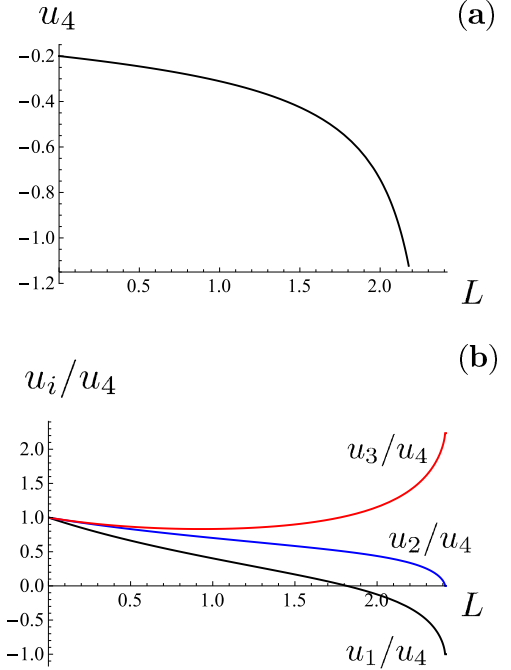


FIG. 5. The numerical solution of Eq. (64) for the RG flow of dimensionless vertices  $u_i$  under the variation of the RG parameter  $L = \log W/E$ , where  $W$  is of order bandwidth and  $E$  is the running energy (or temperature). The initial condition is  $u_i(L=0) = -2\bar{g}$ ,  $i = 1 - 5$ , and we set  $\bar{g} = 0.1$ . (a) The flow of the interaction  $u_4$ . It remains negative, increases by magnitude, and diverges at the critical RG scale  $L_0$ . The divergence indicates that the system develops some form of order. (b) The RG flow of the ratios of the interactions  $u_i/u_4$ . As the RG scale  $L$  approaches the critical value  $L_0$ , the ratios tend to finite values,  $u_1/u_4 = -\gamma_1^f = -1$ ,  $u_2/u_4 = \gamma_2^f = 0$ , and  $u_3/u_4 = \gamma_3^f = \sqrt{5}$ , in agreement with Eq. (70).

Solving it, we obtain

$$\bar{u}_1(L) = \frac{1}{L' - L}, \quad (63)$$

where  $L' = [\bar{u}_1(L=0)]^{-1} = (2\bar{g})^{-1}$ .

The remaining equations from the set (60) reduce to

$$\begin{aligned}\dot{u}_1 &= u_1^2 + u_3^2, \\ \dot{u}_2 &= 2u_1u_2 - 2u_2^2, \\ \dot{u}_3 &= -u_3u_4 + 4u_3u_1 - 2u_2u_3 - u_5u_3, \\ \dot{u}_4 &= -u_4^2 - u_3^2, \\ \dot{u}_5 &= -u_5^2 - u_3^2.\end{aligned}\quad (64)$$

The bare  $u_4(L=0) = u_5(L=0)$ . One can easily check that the running couplings remain equal, i.e.,  $u_4(L) = u_5(L)$ . The numerical solution of Eq. (64) is presented in Fig. 5.

Compared to the fixed trajectory found previously in Ref. [33], the interactions  $u_1$  and  $u_4$  switch their respective roles. In the model with purely repulsive interactions, considered in [33], the interpocket density-density interaction  $u_1 > 0$  gradually increases in the process of pRG flow, while the intrapocket interaction  $u_4$  (initially positive) changes sign

under pRG and gets more and more negative (attractive). The pair hopping term  $u_3$  is positive, and, like  $u_1$ , it gradually increases under pRG. In our model, intrapocket  $u_4$  is negative from the start, and it just gets more negative in the pRG flow. At the same time, inter-pocket  $u_1$  is initially negative, but it changes sign in the pRG flow and keeps increasing as a positive (repulsive) interaction. The pair-hopping term  $u_3$  is positive, and it gets more and more negative under pRG, much like  $u_4$ . As a result, in our case the interactions flow to a different fixed trajectory than that found in Ref. [33].

To analyze the fixed trajectories analytically, it is convenient to introduce  $v_i = -u_i$ ,  $i = 1-4$  and reduce the system of the remaining pRG equations to

$$\begin{aligned}\dot{v}_1 &= -v_1^2 - v_3^2, \\ \dot{v}_2 &= -2v_1v_2 + 2v_2^2, \\ \dot{v}_3 &= 2v_3v_4 + 2v_3v_2 - 4v_3v_1, \\ \dot{v}_4 &= v_4^2 + v_3^2,\end{aligned}\quad (65)$$

with the initial conditions  $v_i(L=0) = 2\bar{g}$ ,  $i = 1-4$ . We search for the fixed trajectory along which the ratios of the couplings tend to finite values. Accordingly, we introduce

$$v_1 = -\gamma_1 v_4, \quad v_2 = \gamma_2 v_4, \quad v_3 = \gamma_3 v_4, \quad (66)$$

where  $\gamma_i$ ,  $i = 1-3$  are constants. Substitution of (66) in (65) yields the set of algebraic equations

$$\begin{aligned}\gamma_1(1 + \gamma_3^2) &= \gamma_1^2 + \gamma_3^2, \\ \gamma_2(1 + \gamma_3^2) &= 2\gamma_2(\gamma_1 + \gamma_2), \\ \gamma_3(1 + \gamma_3^2) &= 2\gamma_3(1 + \gamma_2 + 2\gamma_1).\end{aligned}\quad (67)$$

The trivial fixed trajectory  $\gamma_1 = \gamma_2 = \gamma_3 = 0$  is unstable because the growth of  $v_4$  makes the solution with  $v_3 = 0$  unstable, as follows from the third line in Eq. (65). For the same reason, the solutions  $\gamma_1 = 1, \gamma_2 = 0, \gamma_3 = 0$  and  $\gamma_1 = 0, \gamma_2 = 1/2, \gamma_3 = 0$  are unstable. One can also check that the solution  $\gamma_1 = 1, \gamma_2 = -1/2, \gamma_3 = 0$  is unstable and that there is no solution with  $\gamma_1 = 0, \gamma_2 = 0, \gamma_3 \neq 0$ .

The remaining possibility is that  $\gamma_1 \neq 0$ ,  $\gamma_3 \neq 0$ , and  $\gamma_2 = 0$ . In this case, the set of equations (67) reduces to two equations,

$$\begin{aligned}\gamma_1(1 + \gamma_3^2) &= \gamma_1^2 + \gamma_3^2, \\ (1 + \gamma_3^2) &= 2(1 + 2\gamma_1).\end{aligned}\quad (68)$$

It follows from the second line of Eqs. (68) that  $\gamma_3^2 = 1 + 4\gamma_1$ . The first line of Eqs. (68) can be written as

$$\gamma_3^2(\gamma_1 - 1) = \gamma_1(\gamma_1 - 1). \quad (69)$$

Equation (69) offers two alternatives. The first is  $\gamma_1 = 1$ , and the second is  $\gamma_1 = \gamma_3^2$ . The latter possibility is, however, not viable as in combination with the second line of Eq. (68) it results in the relation  $3\gamma_3^2 + 1 = 0$ , which cannot be satisfied. We therefore have  $\gamma_1 = 1$ , and from the second line of Eq. (68),  $\gamma_3 = \pm\sqrt{5}$ . To fix the sign of  $\gamma_3$ , we note that the unstable fixed trajectory  $\gamma_1 = 1$ ,  $\gamma_2 = 0$ , and  $\gamma_3 = 0$  is the separatrix that cannot be crossed under the pRG flow. In other words, the interaction  $u_3$  maintains its sign under pRG, i.e., it is fixed by the

initial conditions. Since  $v_3(L=0) > 0$ , the fixed trajectory is

$$\gamma_1^f = 1, \quad \gamma_2^f = 0, \quad \gamma_3^f = \sqrt{5}. \quad (70)$$

Let us verify that the fixed trajectory set by Eq. (70) is stable. For this we allow the coefficients  $\gamma_i$ ,  $i = 1-3$  to vary slightly, rewrite the set of pRG equations as the set for  $\gamma_i(L)$ ,

$$\begin{aligned}\dot{\gamma}_1 &= v_4[(\gamma_1^2 + \gamma_3^2) - \gamma_1(1 + \gamma_3^2)], \\ \dot{\gamma}_2 &= v_4[2\gamma_1\gamma_2 + 2\gamma_2^2 - \gamma_2(1 + \gamma_3^2)], \\ \dot{\gamma}_3 &= v_4[2\gamma_3 + 2\gamma_2\gamma_3 + 4\gamma_3\gamma_1 - \gamma_3(1 + \gamma_3^2)],\end{aligned}\quad (71)$$

and linearize Eqs. (71) in small deviations,  $\delta\gamma_i = \gamma_i - \gamma_i^f$ . The set of linear differential equations can be cast into the matrix form

$$\delta\dot{\gamma}_i = \sum_{j=1}^3 \Lambda_{ij} \delta\gamma_j, \quad (72)$$

with

$$\Lambda = -v_4 \begin{bmatrix} 4 & 0 & 0 \\ 0 & 4 & 0 \\ 4\sqrt{5} & 2\sqrt{5} & 10 \end{bmatrix}. \quad (73)$$

We see that  $\Lambda$  is negative-definite. As a result, the fixed trajectory defined by Eq. (70) is stable.

Along the fixed trajectory set by Eq. (70), the fourth equation from Eq. (65) becomes  $\dot{v}_4 = 6v_4^2$ . Assuming that this equation is valid starting already from small  $L$ , we find the solution in the form

$$v_4(L) = \frac{v_4(0)}{1 - 6Lv_4(0)} = \frac{1}{6(L_0 - L)}, \quad (74)$$

where

$$L_0 = \frac{1}{6v_4(0)}. \quad (75)$$

The initial value  $v_4(0) = -u_4(0) = 2\bar{g}$ . Hence

$$L_0 = \frac{1}{12\bar{g}}. \quad (76)$$

Comparing with Eq. (63), we see that  $L_0 < L'$ , hence the couplings  $v_i$  (and  $u_i = -v_i$ ) diverge at a smaller  $L$  (i.e., larger energy) than  $\bar{u}_1$ . Then,  $\bar{u}_1$  can be neglected compared to  $u_i$  near the fixed trajectory.

Summarizing the pRG analysis, we find that for our model there exists one stable fixed trajectory along which

$$\begin{aligned}u_1(L) &= \frac{1}{6(L_0 - L)}, \quad u_3(L) = -\frac{\sqrt{5}}{6(L_0 - L)}, \\ u_4(L) &= u_5(L) = -\frac{1}{6(L_0 - L)},\end{aligned}\quad (77)$$

and the rest of the interactions are either zero, or flow to zero, or increase but at a smaller rate than the interactions listed in Eq. (77).

## V. HIERARCHY OF INSTABILITIES WITHIN pRG

We now reexamine the hierarchy of instabilities using the renormalized, scale-dependent interactions listed in Eq. (77). For this we follow Ref. [33] and earlier functional RG works (Ref. [28]) and obtain and solve the RG equations for the

$$\begin{aligned} \delta\chi_s &= \Gamma_s \text{---} \text{---} \text{---} \Gamma_s \\ &\text{(a)} \\ \delta\chi_c &= \Gamma_c \text{---} \text{---} \text{---} \Gamma_c \\ &\text{(b)} \end{aligned}$$

FIG. 6. Diagrammatic representation of pRG expressions for the susceptibility in the SDW channel (a) and the Cooper channel (b), which give rise to Eqs. (80) and (84), respectively.

vertices  $\Gamma_i$  in different channels, using the running couplings as inputs. We then use the running vertices to compute the susceptibilities in different channels, and we compare the exponents for the susceptibilities  $\chi_j \propto 1/(L_0 - L)_j^{\alpha_j}$ , where  $j$  labels different channels. As in other RG-based approaches, we assume that the instability at  $L = L_0$  will lead to the development of a nonzero mean value of the order parameter, for which  $\alpha_j$  is the largest. We will not present the details of the derivation of RG equations as the computational steps have already been described in Ref. [33]. However, we discuss the computations of the running susceptibility in the Pomeranchuk channels in some more detail.

### A. Magnetism

Within the RPA, the intraorbital SDW does not develop, while the interorbital SDW develops at a lower  $T$  than superconductivity and CDW order. The result of pRG analysis is somewhat different. Namely, real intraorbital order  $s_{1,2}^r$  does not develop because the coupling  $-u_1 - u_3$  remains positive (repulsive) under pRG. But for imaginary intraorbital order  $s_{1,2}^i$  the corresponding dimensionless coupling  $-u_1 + u_3$  becomes positive and grows in the process of RG flow. The RG equation for the vertex function  $\Gamma_s^i$  (introduced in the same way as in Sec. III) is

$$\frac{d\Gamma_s^i}{dL} = (u_1 - u_3)\Gamma_s^i, \quad (78)$$

where  $u_1 = u_1(L)$  and  $u_3 = u_3(L)$  are the running couplings. The boundary condition is  $\Gamma_s^i(L = 0) = \Gamma_s^i(0)$ . The solution of Eq. (78) along the fixed trajectory, i.e., with  $u_1(L)$  and  $u_3(L)$  given by Eq. (77), is

$$\Gamma_s^i = \frac{\Gamma_s^i(0)}{(L_0 - L)^{\beta_s^i}}, \quad \beta_s^i = \frac{1 + \sqrt{5}}{6}. \quad (79)$$

The running susceptibility  $\chi_s^i(L)$  evolves according to

$$\frac{d\chi_s^i}{dL} = [\Gamma_s^i]^2; \quad (80)$$

see Fig. 6(a). Substituting  $\Gamma_s^i(L)$  from Eq. (79) and integrating over  $L$ , we obtain

$$\begin{aligned} \chi_s^i &\propto (L_0 - L)^{-\alpha_s^i}, \\ \alpha_s^i &= 2\beta_s^i - 1 = \frac{\sqrt{5} - 2}{3} \approx 0.08. \end{aligned} \quad (81)$$

The interactions in interorbital SDW channels with real and imaginary order parameters are attractive already at the bare level, and they keep increasing under pRG. The behavior of the corresponding  $\tilde{\Gamma}_s^{r,i}$  is governed by the running  $\tilde{u}_1$ . The latter diverges, but at  $L = L'$ , which is larger than  $L_0$ . As a result, the instability in the intraorbital SDW channel occurs at higher running energy, and hence at a higher temperature.

### B. Superconductivity

We now consider susceptibilities in the superconducting channels. First,  $A_1$  and  $B_1$  channels remain degenerate because the running couplings in these two channels differ by  $\tilde{u}_j$ ,  $j = 3, 4, 5$  [see Eqs. (33) and (34)]. These couplings are zero at the bare level and remain zero under pRG; see Eq. (61). The interaction in the  $s^{+-}$  and  $d^{+-}$  channels is  $u_4 - u_3$ . This interaction is repulsive along the fixed trajectory, hence the corresponding susceptibility does not diverge. The interaction in the  $s^{++}$  and  $d^{++}$  channels is  $u_4 + u_3$ , and this one is negative (attractive) along the fixed trajectory. The RG equation for the SC vertex in the  $s^{++}$  and  $d^{++}$  channels is

$$\frac{d\Gamma_{SC}^{s,d}}{dL} = -(u_4 + u_3)\Gamma_{SC}^{s,d}. \quad (82)$$

Solving this equation, we find

$$\Gamma_{SC}^{s,d} = \frac{\Gamma_{SC}^{s,d}(0)}{(L_0 - L)^{\beta_{SC}^{s,d}}}, \quad \beta_{SC}^s = \beta_{SC}^d = \frac{1 + \sqrt{5}}{6}. \quad (83)$$

The running susceptibilities  $\chi_{SC}^{s,d}(L)$  again evolve according to

$$\frac{d\chi_{SC}^{s,d}}{dL} = [\Gamma_{SC}^{s,d}]^2; \quad (84)$$

see Fig. 6(b). Substituting  $\Gamma_{SC}^{s,d}(L)$  from Eq. (83) and integrating over  $L$ , we obtain

$$\begin{aligned} \chi_{SC}^{s,d} &\propto (L_0 - L)^{-\alpha_{SC}^{s,d}}, \\ \alpha_{SC}^{s,d} &= 2\beta_{SC}^{s,d} - 1 = \frac{\sqrt{5} - 2}{3} = \alpha_{SC}^i. \end{aligned} \quad (85)$$

We see that the susceptibilities in the  $s^{++}$  and  $d^{++}$  channels have the same exponents as the susceptibility in the intraorbital SDW channel with imaginary order parameter. For the  $B_2$  channel, the tendency toward pairing is suppressed at low energies because  $\tilde{u}_{4,5}$  and  $\tilde{u}_{4,5}$  flow to zero.

### C. CDW order

The same analysis as in the previous two subsections shows that the susceptibility for the real intraorbital order parameter  $\delta_{1,2}^r$  diverges as  $L$  approaches  $L_0$ , while the susceptibilities in other CDW channels do not diverge. The divergent CDW susceptibility scales as

$$\chi_c^r \propto (L_0 - L)^{-\alpha_c^r}, \quad (86)$$

where  $\alpha_c^r = (\sqrt{5} - 2)/3$ . This exponent is the same as  $\alpha_{SC}^{s,d}$  and  $\alpha_s^i$ , i.e., within the RG the susceptibilities in all these channels scale with each other. The susceptibilities in the interorbital CDW channels remain regular, i.e., the corresponding order parameters do not develop at  $L = L_0$ .

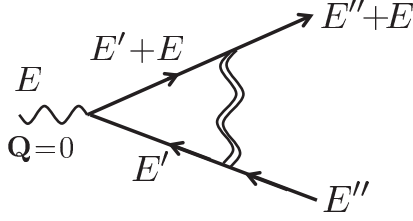


FIG. 7. The diagrammatic representation of the lowest-order vertex renormalization in the Pomeranchuk channel. The double wavy line represents the running interaction  $U_i(L)$ . The external  $E$  and  $E'' \sim E$  can be regarded either as frequencies in  $T = 0$  calculations or as a temperature. In the first case, the integral over internal  $E'$  does not vanish because the running interaction is also a function of  $E'$ , and it is equal to the density of states  $N_F$  times the coupling at a scale  $E$ . In the second case, the interaction is treated as static, but the convolution of the two fermion propagators is again nonzero and equal to the density of states  $N_F$ .

#### D. Pomeranchuk order

Within the RPA, the instability in any of the Pomeranchuk channels develops only when the interaction exceeds a certain threshold. This is a consequence of the fact that the renormalization of the Pomeranchuk vertex is determined by the convolution of the two fermion propagators at vanishing transferred momentum and zero transferred frequency. This convolution gives a constant (equal to the density of states at the Fermi level), but not a logarithm.

Within pRG, we need to evaluate the vertex at a running frequency. The triple vertex, shown in Fig. 7, depends on two external frequencies,  $E$  and  $E''$  (the third one is  $E'' + E$  by frequency conservation). To obtain susceptibility, we will need to integrate over  $E''$ . We assume and then verify that relevant  $E''$  are comparable to  $E$ .

If we reevaluate the convolution of the two propagators at a finite  $E$  and  $Q = 0$ , we obtain that the result vanishes, because the poles in the two fermionic propagators are in the same half-plane of a complex frequency. Does this imply that the Pomeranchuk vertex is not renormalized within the RG? We argue that it does not, and the Pomeranchuk vertex does flow under the RG. The reason is that to obtain vertex renormalization, we actually need to compute the product of the two fermionic propagators and the interaction. This combination is expressed via the convolution of the two fermionic propagators at a finite  $E$  and  $Q = 0$  only if the interaction is static. But the running interaction is not a constant but rather a function of the running fermionic frequency  $E'$  and also of external  $E'' \sim E$ . As a consequence, when we compute the renormalization of the Pomeranchuk vertex at a given energy  $E$ , we need to evaluate the momentum and frequency integral of the product of the two propagators and the running interaction (see Fig. 7):

$$I(E) = \int d^2k dE' \frac{1}{iE' - \epsilon_k} \frac{1}{i(E' + E) - \epsilon_k} U_j(E, E'), \quad (87)$$

where  $U_j$  is one of the interactions (see Fig. 7). One can verify that, to logarithmic accuracy, the dependence of the interaction  $U_j(E, E')$  on  $|E|$  and  $|E'|$  can be cast as the dependence on

$L = \log W/(|E| + |E'|)$ . Because  $U_j(E, E')$  has a nonanalytic dependence on the running  $E'$ , the integrand in (87) contains branch cuts in addition to the poles, and the branch cuts are present in both half-planes of complex  $E'$ . In this situation, it is more convenient to first evaluate the integral over  $d^2k$  and then over  $dE'$ . For this, we subtract from  $U_j(E, E')$  its constant value at  $E, E' = W$ . This does not change  $I(E)$  because, as we just said, the term we subtract gives zero contribution to  $I(E)$ . The integrand in (87) with  $U_j(E, E') - U_j(W)$  converges, and the integration can be done in any order. Taking for definiteness fermions near an electron pocket, transforming from the integration over  $d^2k$  to integration over  $d\epsilon_k$  via  $\int d^2k = N_F \int_{-E_F}^W d\epsilon_k$ , and integrating over  $\epsilon_k$  first, we obtain for positive  $E > E_F$ ,

$$I(E) \sim N_F \int_{E_F}^E \frac{dE'}{E} [U_j(E, E') - U_j(W)], \quad (88)$$

or, in logarithmic variables,

$$I(L) \sim N_F \int_{L-\log 2}^L e^{L-L'} [U_j(L') - U_j(W)] \sim u_j(L). \quad (89)$$

Evaluating this integral to logarithmic accuracy, we find that one-loop renormalization of the Pomeranchuk vertex  $\Gamma_{\text{ph}}(L)$  yields  $\Gamma_{\text{ph}}(L) \propto u_j(L)$ , i.e., the vertex at a scale  $L$  is proportional to the running interaction at the same scale  $L$ .

Alternatively, we can view the RG energy variable  $E$  as a temperature and consider how the couplings vary as one progressively integrates out fluctuations at a higher  $T$ . In this approach, the susceptibilities in all channels are the static ones ( $E = 0$ ), but taken at a finite  $T$ . The integration over  $E'$  in (87) now has to be replaced by the summation over Matsubara frequencies. A static interaction can be taken outside the frequency summation, but the latter now gives a finite result because regularization by a finite  $T$  yields the same result—the density of states  $N_F$ —as the evaluation of the convolution of the two  $G$ 's at  $T = 0$ ,  $E = 0$ , and  $Q \rightarrow 0$ . Furthermore, relevant internal  $E'$  is of order  $T$ . Hence, the vertex at a given  $T$  is proportional to the interaction at the same  $T$ , i.e., in logarithmic variables we have the same dependence  $\Gamma_{\text{ph}}(L) \propto u_j(L)$  as in  $T = 0$  analysis with frequency  $E$  as the running variable.

Another consequence of the pRG flow of the couplings is that the interplay between the running interactions  $u_j(L)$  is different from that between the bare interactions, chiefly because  $u_1(L)$  changes its sign in the process of RG flow and becomes positive, i.e., attractive in  $A_{1g}$  and  $B_{1g}$  Pomeranchuk channels.

We now sum up the ladder series of renormalizations of  $\Gamma_{\text{ph}}$  [see Fig. 8(a)]. These are the same series as we summed up for the SDW and SC vertices. The summation leads to the same matrix equations for the full vertices  $\Gamma_{\text{ph}; B_i}^{f,d}(L)$  as in the RPA analysis of Pomeranchuk instabilities, Eq. (51), but now  $u_i$  are the running interactions. Along the fixed trajectory, we obtain

$$M_{\text{ph}; B_1} = -2 \begin{bmatrix} u_4 & 2u_1 \\ 2u_1 & u_5 \end{bmatrix}. \quad (90)$$

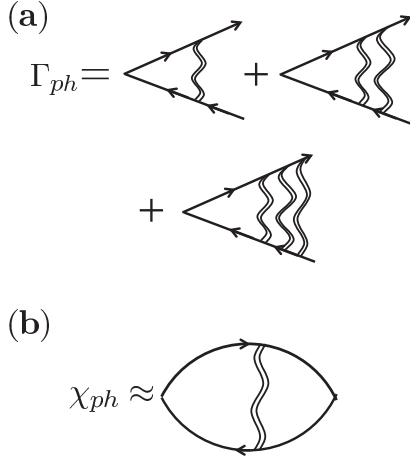


FIG. 8. (a) Series of ladder diagrams for the vertex function in the Pomeranchuk channel. Compared to the diagram in Fig. 7, these diagrams account for the shift of the critical  $L$  from  $L = 0$  to  $L_{ph} = L_0 - 1$ . This shift is beyond logarithmic accuracy, and we neglect it when we compare Pomeranchuk and other channels. (b) The contribution to the Pomeranchuk susceptibility to first order in the running coupling. The logarithmic enhancement of the Pomeranchuk susceptibility is due to  $1/(L_0 - L)$  scaling of the interaction at the running pRG scale  $L$ .

Substituting  $u_j(L)$  from Eq. (77), we reexpress (90) as

$$M_{ph;B_1} = \frac{1}{3(L_0 - L)} \begin{bmatrix} 1 & -2 \\ -2 & 1 \end{bmatrix}. \quad (91)$$

The two eigenvalues of this matrix are

$$\lambda_{B_1,++} = -\frac{1}{3(L_0 - L)}, \quad \lambda_{B_1,+-} = \frac{1}{(L_0 - L)}. \quad (92)$$

We remind the reader that notations  $++$  and  $+-$  refer to  $B_1$  ( $d$ -wave) order parameters  $n_{xz}-n_{yz}$  with the same (opposite) sign on the hole and electron pockets. It follows from Eq. (92) that the Pomeranchuk instability is the  $d^{+-}$  channel. This is different from the RPA, where we found the leading instability in the  $d^{++}$  channel. The discrepancy with the RPA is a consequence of the sign reversal of the interaction  $u_1(L)$  in the process of pRG flow.

The instability toward  $d^{+-}$  nematic order occurs when  $\lambda_{ph;+-} = 1$ , i.e., at  $L_{ph} = L_0 - 1$ . This difference, however, is beyond logarithmic accuracy and we neglect it, i.e., we approximate  $L_{ph}$  by  $L_0$ . In the diagrammatic approach, this corresponds to keeping only the leading term in the ladder series for  $\Gamma_{ph;B_1}^{f,d}(L)$ ; see Fig. 8(b).

More important is the fact that near the instability, the Pomeranchuk vertex scales as

$$\Gamma_{ph;B_1}^{f,d}(L) \propto \frac{1}{L_0 - L}, \quad (93)$$

i.e., the corresponding  $\beta_{ph} = 1$ , while for other channels  $\beta$  is close to  $1/2$ .

Using the same reasoning in the computation of the susceptibility in the  $B_1$  Pomeranchuk channel, we find

$$\chi_{ph;B_1}(L) \propto \frac{1}{L_0 - L}, \quad (94)$$

i.e., the exponent for the Pomeranchuk susceptibility in the  $B_1$  channel is  $\alpha_{ph} = 1$ , much larger than  $\alpha = 0.08$  in the SDW, CDW, and  $s$ - and  $d$ -SC channels. This difference in the numbers is important because compared to other susceptibilities, the one in the Pomeranchuk channel contains an additional factor of a running coupling  $u(L)$  due to the absence of the logarithm in the vertex renormalization. At some distance from  $L = L_0$ ,  $u(L) \sim 1/L_0$  is small, hence  $\chi_{ph;B_1}$  is parametrically smaller than other susceptibilities. If the exponents in the Pomeranchuk and other channels were similar in magnitude,  $\chi_{ph;B_1}$  would exceed susceptibilities in other channels only at  $L$  near  $L_0$ , where  $u(L) \geq 1$ , and the accuracy of one-loop pRG is questionable. Because all other  $\alpha$  are small and  $\alpha_{ph;B_1} = 1$ ,  $\chi_{ph;B_1}$  becomes larger than the susceptibilities in other channels at much larger distance from  $L_0$ , when one-loop pRG is likely still valid.

We refrain from discussing the susceptibility in the  $A_1$  Pomeranchuk channel because, as we said, this susceptibility does not actually diverge. The interactions in  $A_2$  and  $B_2$  Pomeranchuk channels flow to zero under pRG, i.e., the corresponding susceptibilities do not diverge.

We note that the Pomeranchuk order changes the shape of the Fermi surface, but it leaves fermionic excitations gapless. This leaves the possibility that superconductivity emerges at a lower temperature inside the nematic phase, as happens in FeSe. In our model, the behavior in the nematic phase may be even more complex as the susceptibilities in SC, SDW, and CDW channels are expected to continue to grow below the nematic transition. These three channels compete for the secondary instability, and the outcome of this competition depends on the details of the electronic structure, such as the degree of nesting between electron and hole pockets and the ratio of hole and electron masses. A detailed study of this competition is beyond the scope of this work.

## VI. DISCUSSION

In this paper, we performed a detailed study of potential two-fermion instabilities in a model of FeSCs with the interaction tailored to favor  $C_4$ -breaking orbital order. In contrast with the two-orbital model with the same interaction considered in earlier works, we used the correct four-pocket band structure with two hole pockets at the center of the BZ and two electron pockets at its boundaries. We kept the orbital content of low-energy excitations, which allowed us to include orbital fluctuations along with SDW, CDW, and SC fluctuations. We have shown that the interplay between different interaction channels has a substantial effect on the hierarchy of the ordering tendencies.

We first analyzed the model within the RPA, which neglects the interplay between different channels. We found that the highest- $T$  instabilities at weak coupling are in  $s^{++}$  and  $d^{++}$  SC channels ( $s$ -wave and  $d$ -wave with no sign change of the gap between hole and electron pockets), and in an intraorbital CDW channel with transferred momenta  $(0, \pi)$  or  $(\pi, 0)$ . The instability temperature is the same in all three channels. The sign-preserving SC state wins over sign-changing states ( $s^{+-}$  and  $d^{+-}$ ) because in our model intraorbital interaction is attractive. The degeneracy between  $s^{++}$  and  $d^{++}$  channels is a consequence of the absence of the Hund coupling  $J'$ , which

would give rise to the tunneling of Cooper pairs of electrons on  $d_{xz}$  orbitals into Cooper pairs on  $d_{yz}$  orbitals and vice versa.

There is also attractive interaction in interorbital SDW and CDW channels. The instability temperature is the same in both channels, but it is lower than that in the three leading channels. In addition, there is attractive interaction in  $B_{1g}$ ,  $A_{2g}$ , and  $B_{2g}$  Pomeranchuk channels, but the instability there occurs only when the coupling exceeds a certain threshold. The threshold value is the smallest in  $B_{1g}$  channel.

We next studied the effect of coupling between different channels. We applied the RG technique, we obtained and solved the set of parquet RG equations for the interactions, and we identified the stable fixed trajectory as the asymptotic solution of these equations. On a fixed trajectory, the ratio of any two interactions is just a number. We found that the fixed trajectory in our model is notably distinct from the one obtained for the model with intraorbital and interorbital repulsion. In the latter case, the intrapocket interactions flip the sign before the system reaches the fixed trajectory. This turns intrapocket repulsion into an attraction. The interaction describing the interpocket tunneling of Cooper pairs remains attractive and becomes the strongest under pRG. This gives rise to  $s^{++}$  superconductivity. The interplay between different couplings is such that SC wins over intraorbital SDW, but the SC susceptibility gets weakened by the competition and may lose to  $d$ -wave Pomeranchuk order.

In the model that we considered here, intrapocket interactions and the interpocket Cooper pair tunneling are attractive at the bare level and remain attractive in the process of pRG flow, while interpocket density-density interaction flips sign under pRG from attraction to repulsion. As a consequence, four channels are degenerate along the fixed trajectory in the sense that the corresponding susceptibilities all diverge at the same energy (temperature) and with the same exponent. These four are  $s^{++}$  and  $d^{++}$  SC channels, an intraorbital CDW channel, and an intraorbital SDW channel, all with real order parameter. Due to the strong competition between that many channels, the exponent for the susceptibilities is quite small,  $\alpha = 0.08$ , i.e., the four susceptibilities barely diverge at the critical RG scale. Meanwhile, the  $d$ -wave Pomeranchuk channel (the one with the  $C_4$ -breaking orbital order parameter  $n_{xz}-n_{yz}$ ) remains attractive during pRG flow, and the exponent for the  $d$ -wave Pomeranchuk susceptibility is  $\alpha = 1$ . At intermediate RG scales, Pomeranchuk susceptibility is smaller than the ones in four other singular channels because of the absence of a logarithm in the particle-hole polarization bubble at zero momentum transfer. But near the critical RG scale  $L = L_0$ , Pomeranchuk susceptibility is the largest because of the larger exponent  $\alpha$ . Because of the large numerical difference between  $\alpha = 1$  in the  $d$ -wave Pomeranchuk channel and  $\alpha = 0.08$  in other channels, the susceptibility in the Pomeranchuk channels becomes the largest already at a substantial distance from the critical RG scale  $L_0$ , when the one-loop pRG approach is under control in the sense that two-loop corrections are numerically small. The outcome is that in the model that we considered in this work, the leading candidate for the instability already at weak coupling is a spontaneous orbital order. The verification of this result in numerical studies is called for.

From a physics perspective, the microscopic mechanism for the Pomeranchuk order in the model of Eq. (5) is twofold. First, growing CDW fluctuations not only boost the attraction in the current (imaginary) intraorbital SDW channel and in  $s^{+}$ - and  $d$ -wave superconducting channels, but they also boost attractive interaction in the  $d$ -wave Pomeranchuk channel. Second, SC and SDW channels compete with the CDW channel, and this competition reduces SDW and superconducting susceptibilities. The  $d$ -wave Pomeranchuk channel does not compete with other channels, and the susceptibility in this channel is not reduced. This is why the exponent in this channel is larger than those in the other channels. We also emphasize that pRG analysis goes beyond the RPA. In the RPA, there is an instability in the  $d$ -wave Pomeranchuk channel in the model of Eq. (5), but it holds only when  $g$  exceeds the critical value  $g_c$ , and it is always secondary to superconductivity. The pRG analysis includes two effects not present in the RPA: (i) the boost of the interaction in the Pomeranchuk channel by CDW fluctuations, and (ii) the reduction of the susceptibility in the superconducting channel due to competition with the CDW.

An obvious issue is how sensitive are our results to the modification of the Hamiltonian, particularly the modification of the interaction in Eq. (5), of the degree of nesting and the value of the chemical potential in the electronic structure, and of the strength of the interaction. In this regard, we make a few observations. First, in the pRG approach, nesting (by which we mean near equal size of hole and electron pockets) does not play the crucial role. All that matters for pRG is the opposite sign of the dispersion of excitations near hole and electron pockets. Second, the pRG flow holds at energies between the bandwidth and the Fermi energy, and as such it is not sensitive to the details of the electronic structure at energies smaller than  $E_F$ . In this respect, variations of the chemical potential over an energy range smaller than the Fermi energy will not affect the pRG flow. The variation of the ratio of hole and electron masses also does not affect the behavior of the couplings along the fixed RG trajectory and the hierarchy of instabilities. Third, in any one-loop RG-based study, there are two assumptions: (i) that the channel for the leading instability gets selected already within the applicability range of RG (i.e., at energies above  $E_F$ ), and (ii) that the terms beyond one-loop RG do not affect this selection. The larger the bare coupling is [ $g$  in Eq. (5)], the more important are the terms beyond one-loop RG. Neither we nor other groups analyzing the RG flow in multiorbital systems went beyond one-loop RG simply because one-loop RG equations are already complex enough. Whether the RG results remain valid at  $g$  comparable to the bandwidth should be addressed by comparing the RG phase diagram with the results of numerical studies. We also note that the huge difference between the exponents in the Pomeranchuk channel and in other channels in our model is a guarantee that the Pomeranchuk channel wins even in a more complex model, where SC, SDW, and CDW susceptibilities become nonequal, and one of the corresponding exponents become larger. Indeed, this holds only as long as all exponents remain substantially smaller than 1. If this is not the case, our reasoning breaks down.

A more subtle aspect, which is not fully understood at the moment, is whether the fact that CDW, SDW, and SC orders all may potentially break  $C_4$  symmetry plays a role in the

system's selection of the  $C_4$  breaking Pomeranchuk order as the leading instability. Indeed, the stripe CDW and SDW break  $C_4$ , and the degeneracy between  $s$ - and  $d$ -wave SC orders opens the way to the  $s + id$  state, which also breaks  $C_4$ . At the same time, whether or not CDW or SDW order is a stripe or a checkerboard can be determined only by analyzing the interplay between fourth-order terms in SDW and CDW order parameters. Such terms are of eighth-order in fermions and are beyond the one-loop RG.

## ACKNOWLEDGMENTS

We thank G. Blumberg, L. Classen, R. M. Fernandes, V. K. Thorsmølle, O. Vafek, and R. Xing for useful discussions. M.K. acknowledges the support by the Israel Science Foundation, Grant No. 1287/15, and NSF Grant No. DMR-1506668. A.V.C. acknowledges the support by the Office of Basic Energy Sciences, U.S. Department of Energy, under Award No. DE-SC0014402.

- 
- [1] D. C. Johnston, *Adv. Phys.* **59**, 803 (2010).
  - [2] Z. P. Yin, K. Haule, and G. Kotliar, *Nat. Mater.* **10**, 932 (2011).
  - [3] P. Dai, J. Hu, and E. Dagotto, *Nat. Phys.* **8**, 709 (2012).
  - [4] A. V. Chubukov, *Annu. Rev. Condens. Matter Phys.* **3**, 57 (2012).
  - [5] R. M. Fernandes, A. V. Chubukov, and J. Schmalian, *Nat. Phys.* **10**, 97 (2014).
  - [6] I. Gallais and I. Paul, *C. R. Phys.* **17**, 113 (2016).
  - [7] R. M. Fernandes and J. Schmalian, *Supercond. Sci. Technol.* **25**, 084005 (2012).
  - [8] S. Lederer, Y. Schattner, E. Berg, and S. A. Kivelson, *Phys. Rev. Lett.* **114**, 097001 (2015).
  - [9] Y. Yamakawa, S. Onari, and H. Kontani, *Phys. Rev. X* **6**, 021032 (2016).
  - [10] P. Chandra, P. Coleman, and A. I. Larkin, *Phys. Rev. Lett.* **64**, 88 (1990).
  - [11] C. Fang, H. Yao, W. F. Tsai, J. P. Hu, and S. A. Kivelson, *Phys. Rev. B* **77**, 224509 (2008).
  - [12] C. Xu, M. Muller, and S. Sachdev, *Phys. Rev. B* **78**, 020501 (2008).
  - [13] Y. Qi and C. Xu, *Phys. Rev. B* **80**, 094402 (2009).
  - [14] R. M. Fernandes, L. H. VanBebber, S. Bhattacharya, P. Chandra, V. Keppens, D. Mandrus, M. A. McGuire, B. C. Sales, A. S. Sefat, and J. Schmalian, *Phys. Rev. Lett.* **105**, 157003 (2010).
  - [15] R. M. Fernandes, A. V. Chubukov, J. Knolle, I. Eremin, and J. Schmalian, *Phys. Rev. B* **85**, 024534 (2012).
  - [16] H. Yamase and R. Zeyher, *New J. Phys.* **17**, 073030 (2015).
  - [17] L. Fanfarillo, A. Cortijo, and B. Valenzuela, *Phys. Rev. B* **91**, 214515 (2015).
  - [18] S.-H. Baek, D. V. Efremov, J. M. Ok, J. S. Kim, J. van den Brink, and B. Buchner, *Nat. Mater.* **14**, 210 (2015).
  - [19] F. Krüger, S. Kumar, J. Zaanen, and J. van den Brink, *Phys. Rev. B* **79**, 054504 (2009).
  - [20] C.-C. Lee, W.-G. Yin, and W. Ku, *Phys. Rev. Lett.* **103**, 267001 (2009).
  - [21] C. C. Chen, J. Maciejko, A. P. Sorini, B. Moritz, R. R. P. Singh, and T. P. Devereaux, *Phys. Rev. B* **82**, 100504(R) (2010).
  - [22] W. Lv, F. Krüger, and P. Phillips, *Phys. Rev. B* **82**, 045125 (2010).
  - [23] S. Onari and H. Kontani, *Phys. Rev. Lett.* **109**, 137001 (2012).
  - [24] H. Yamase and R. Zeyher, *Phys. Rev. B* **88**, 180502(R) (2013).
  - [25] H. Yamase and R. Zeyher, *Phys. Rev. B* **88**, 125120 (2013).
  - [26] A. V. Chubukov and R.-Q. Xing, *Phys. Rev. B* **93**, 165141 (2016).
  - [27] P. T. Dumitrescu, M. Serbyn, R. T. Scalettar, and Vishwanath, *arXiv:1512.08523*.
  - [28] C. Platt, C. Honerkamp, and W. Hanke, *New J. Phys.* **11**, 055058 (2009).
  - [29] A. V. Chubukov, D. V. Efremov, and I. Eremin, *Phys. Rev. B* **78**, 134512 (2008).
  - [30] A. V. Chubukov, *Physica C* **469**, 640 (2009).
  - [31] S. Maiti and A. V. Chubukov, *Phys. Rev. B* **82**, 214515 (2010).
  - [32] C. Platt, W. Hanke, and R. Thomale, *Adv. Phys.* **62**, 453 (2013).
  - [33] A. V. Chubukov, M. Khodas, and R. M. Fernandes, *arXiv:1602.05503*.
  - [34] V. Cvetkovic and O. Vafek, *Phys. Rev. B* **88**, 134510 (2013).
  - [35] A. B. Vorontsov, M. G. Vavilov, and A. V. Chubukov, *Phys. Rev. B* **81**, 174538 (2010).